Received: 28 August 2018 | Revised: 7 December 2018 | Accepted: 21 December 2018

DOI: 10.1002/hbm.24507

WILEY

RESEARCH ARTICLE

Amyloid burden accelerates white matter degradation in cognitively normal elderly individuals

Ashwati Vipin[1] | Kwun Kei Ng[1] | Fang Ji[1] | Hee Youn Shim[1] | Joseph K. W. Lim[1] | Ofer Pasternak[2] | Juan Helen Zhou[1,3] | for the Alzheimer's Disease Neuroimaging Initiative[†]

[1]Center for Cognitive Neuroscience, Neuroscience and Behavioural Disorders Program, Duke-National University of Singapore Graduate Medical School, Singapore

[2]Departments of Psychiatry and Radiology, Brigham and Women's Hospital, Harvard Medical School, Boston, Massachusetts

[3]Clinical Imaging Research Centre, the Agency for Science, Technology and Research and National University of Singapore, Singapore

Correspondence
Juan Helen Zhou, PhD, Duke-NUS Medical School, 8 College Road, #06-15, Singapore 169857.
Email: helen.zhou@duke-nus.edu.sg

Funding information
Ministry of Health, Singapore, Grant/Award Number: Duke-NUS Medical School Signature Research Program; National Medical Research Council, Grant/Award Number: NMRC0088/2015; Biomedical Research Council, Singapore, Grant/Award Number: BMRC 04/1/36/372; National Institute of Biomedical Imaging and Bioengineering; National Institute on Aging; Department of Defense, Grant/Award Number: W81XWH-12-2-0012; National Institutes of Health, Grant/Award Numbers: P41 EB015902, awarded to OP; Alzheimer's Disease Neuroimaging Initiative, Grant/Award Number: U01 AG024904

Abstract

Alterations in parietal and temporal white matter microstructure derived from diffusion tensor imaging occur in preclinical and clinical Alzheimer's disease. Amyloid beta (Aβ) deposition and such white matter alterations are two pathological hallmarks of Alzheimer's disease. However, the relationship between these pathologies is not yet understood, partly since conventional diffusion MRI methods cannot distinguish between cellular and extracellular processes. Thus, we studied Aβ-associated longitudinal diffusion MRI changes in Aβ-positive (N = 21) and Aβ-negative (N = 51) cognitively normal elderly obtained from the Alzheimer's Disease Neuroimaging Initiative dataset using linear mixed models. Aβ-positivity was based on Alzheimer's Disease Neuroimaging Initiative amyloid-PET recommendations using a standardized uptake value ratio cut-off of 1.11. We used free-water imaging to distinguish cellular and extracellular changes. We found that Aβ-positive subjects had increased baseline right uncinate fasciculus free-water fraction (FW), associated with worse baseline Alzheimer's disease assessment scale scores. Furthermore, Aβ-positive subjects showed faster decrease in fractional anisotropy (FW-corrected) in the right uncinate fasciculus and faster age-dependent right inferior longitudinal fasciculus FW increases over time. Right inferior longitudinal fasciculus FW increases were associated with greater memory decline. Importantly, these results remained significant after controlling for gray and white matter volume and hippocampal volume. This is the first study to illustrate the influence of Aβ burden on early longitudinal (in addition to baseline) white matter changes in cognitively normal elderly individuals at-risk of Alzheimer's disease, thus underscoring the importance of longitudinal studies in assessing microstructural alterations in individuals at risk of Alzheimer's disease prior to symptoms onset.

KEYWORDS

Alzheimer's disease, amyloid beta, at-risk cognitively normal elderly, diffusion tensor imaging, free-water correction, longitudinal study

1 | INTRODUCTION

Extracellular deposits of amyloid beta (Aβ) protein are neuropathological hallmarks of Alzheimer's disease (AD) and are elevated in approximately 30% of clinically normal adults (Rabinovici & Jagust, 2009; Sojkova & Resnick, 2011). Aβ deposition can be measured using amyloid positron emission tomography (PET) imaging (Sojkova & Resnick, 2011) or cerebrospinal fluid markers $A\beta_{42}$ assay (McKhann et al., 2011). Asymptomatic individuals with significant Aβ deposition are classified as being at-risk of AD (Jack Jr. & Vemuri, 2018; Sperling

Abbreviations: AD, Alzheimer's disease; ADAS, Alzheimer's disease assessment scale; ADNI, Alzheimer's Disease Neuroimaging Initiative; Aβ, amyloid beta; DA, axial diffusivity; DAt, tissue axial diffusivity; DR, radial diffusivity; DRt, tissue radial diffusivity; DTI, diffusion tensor MRI; FA, fractional anisotropy; FAt, tissue fractional anisotropy; FW, free water; ILF, inferior longitudinal fasciculus; RILF, right inferior longitudinal fasciculus; RUNC, right uncinate fasciculus; TRACULA, TRActs Constrained by UnderLying Anatomy; UNC, uncinate fasciculus.

[†]Data used in preparation of this article were obtained from the Alzheimer's Disease Neuroimaging Initiative (ADNI) database (adni.loni.usc.edu). As such, the investigators within the ADNI contributed to the design and implementation of ADNI and/or provided data but did not participate in analysis or writing of this report. A complete listing of ADNI investigators can be found at: http://adni.loni.usc.edu/wp-content/uploads/how_to_apply/ADNI_Acknowledgement_List.pdf

et al., 2011). Recent models hypothesize that Aβ deposition is closely followed in time by white matter microstructural abnormalities in the at-risk cognitively normal elderly stage (Jack Jr. et al., 2013; Sachdev, Zhuang, Braidy, & Wen, 2013). Supporting this hypothesis are diffusion tensor MRI (DTI) studies in the asymptomatic elderly and mild cognitive impairment, finding microstructural alterations in parietal and temporal white matter fibers, including the uncinate fasciculus and parahippocampal cingulum (Englund, Brun, & Alling, 1988; Remy, Vayssiere, Saint-Aubert, Barbeau, & Pariente, 2015; Rieckmann et al., 2016; Wang et al., 2012). However, evidence has not been conclusive with some illustrating reduced fractional anisotropy or white matter integrity in the fornix and corpus callosum associated with Aβ burden (Chao et al., 2013; Gold et al., 2014; Melah et al., 2016) while others report higher fractional anisotropy and axial diffusivity in the hippocampal cingulum, corpus callosum, and superior longitudinal fasciculus in cognitively normal older individuals (Adluru et al., 2014; Molinuevo et al., 2014; Racine et al., 2014). Longitudinal assessments, ideally sampling individuals at the same stage and subtype of AD, are thus needed to elucidate such complex associations between Aβ burden and white matter microstructure in the asymptomatic preclinical phase of AD.

Such high variability of DTI findings in the clinically normal elderly could also be attributed to the lack of specificity of DTI measures to various biological pathologies, such as axonal degeneration, demyelination, extracellular volume changes (Assaf & Pasternak, 2008), aging-related brain atrophy (Ge et al., 2002), and inflammation possibly related with Aβ deposition (Perez-Nievas et al., 2013). Recently, the free-water (FW) imaging method has been developed to eliminate partial volume with freely diffusing extracellular water molecules in diffusion-weighted MRI (Pasternak, Sochen, Gur, Intrator, & Assaf, 2009; Pasternak, Westin, Dahlben, Bouix, & Kubicki, 2015). The method allows separately identifying extracellular changes affecting the FW measure, from cellular changes influencing the FW-corrected fractional anisotropy measure (FAt). Accordingly FW changes can be sensitive to extracellular processes including atrophy, neuroinflammation and blood–brain barrier permeability modulation (Ji et al., 2017; Pasternak et al., 2012; Perez-Nievas et al., 2013), while FAt changes are more sensitive to alterations in white matter microstructural organization (Lyall et al., 2017; Montal et al., 2017; Pasternak et al., 2012, 2015).

Although cognitively normal elderly individuals exhibiting AD pathologies have been an important population for disease intervention and understanding (Palmqvist et al., 2017; Rieckmann et al., 2016), a few research gaps remain to be addressed. Little is known about the Aβ burden influence on the temporal progression of white matter measures in the asymptomatic preclinical phases of AD (Maier-Hein et al., 2015; Metzler-Baddeley et al., 2012; Rieckmann et al., 2016; Sachdev et al., 2013). Moreover, while we and others have indicated associations between white matter microstructure and cognition in the cognitively normal elderly (Hong et al., 2015; Lovden et al., 2014; Vernooij et al., 2009), it is unclear if these correlations are driven by at-risk asymptomatic elderly individuals. Understanding whether aging modulates the interaction between Aβ burden and white matter measures is another important un-answered gap toward better understanding of AD progression.

To fill these gaps, the present study aimed to compare longitudinal white matter measures in asymptomatic elderly, with and without Aβ burden, from the Alzheimer's disease neuroimaging initiative (ADNI) database. We used linear mixed modeling to assess the influence of Aβ burden on FW-corrected white matter microstructure and FW. We hypothesize that participants with significant Aβ burden (Aβ-positive) would show increased FW and reduced FAt in parietal and temporal fibers compared with those without significant Aβ burden (Aβ-negative) at baseline and/or over time. We also sought to test whether these white matter abnormalities related to cognitive decline at baseline and over time in at-risk cognitively normal elderly individuals.

2 | METHODS

All imaging, demographical, and neuropsychological data used in the preparation of this article were obtained from the Alzheimer's Disease Neuroimaging Initiative (ADNI) database (adni.loni.usc.edu). The ADNI was launched in 2003 as a public–private partnership, led by Principal Investigator Michael W. Weiner, MD. The primary goal of ADNI has been to test whether serial magnetic resonance imaging (MRI), positron emission tomography (PET), other biological markers, and clinical and neuropsychological assessment can be combined to measure the progression of mild cognitive impairment (MCI) and early Alzheimer's disease (AD). For complete information, see www.adni-info.org.

2.1 | Participants

Longitudinal data were obtained from the ADNI2 dataset. Eighty-four cognitively normal older adults were first identified based on the inclusion, exclusion, and diagnostic criteria in the ADNI2 procedures manual (Alzheimer Disease Neuroimaging Initiative, 2008). Following quality control, out of these 84 participants, 72 (43 Females; mean age = 73.72 years, SD = 5.65 years at baseline, Table 1) cognitively normal participants were included in our study. Based on the ADNI criteria, cognitively normal individuals were required to be free of subjective memory concerns, have a score within the normal range on the WMS Logical Memory II (≥9 for 16 years of education and above), have a mini-mental state examination score between 24 and 30, and a clinical dementia rating of 0. Individual participants were chosen if they underwent at least two time points of both neuroimaging and neuropsychological assessments, which included: mini-mental state examination, clinical dementia rating, Alzheimer's Disease Assessment Scale (ADAS), and composite measures for executive function and memory. They were also required to have a mini-mental state examination score of 26 or greater at every time point and maintained a stable diagnosis over at least two consecutive time points. It should be noted that out of all the cognitively normal elderly participants in our study, only five participants progressed to the mild cognitive impairment stage at follow-up time points. Two of these subjects were Aβ -positive at baseline while three were Aβ -negative. Importantly data at the time point of conversion and time points following conversion was not included in our study and analyses. Participants that did not pass the motion criteria for T1 images and region-specific quality control for DTI images were excluded. To minimize the potential confounding effect of scanner sites/types, images obtained only from 3 T

TABLE 1 Demographic and cognitive characteristics between cognitively normal elderly Aβ-positive and Aβ-negative participants

	Aβ −ve (*N* = 51)	Aβ +ve (*N* = 21)	*p*-value; T-score
Baseline age	72.21 (6.05)	73.71 (3.93)	0.22; −1.24
Gender	25/26	4/17	0.03; Fisher's exact test
Right-handedness	46/5	19/2	1.00; Fisher's exact test
Education years	16.78 (2.58)	15.33 (2.76)	0.046; 2.06
Baseline amyloid burden	1.01 (0.05)	1.27 (0.16)	<0.0001; −7.33
ADAS	7.37 (3.71)	9.42 (5.26)	0.114; −1.63
MMSE	29.00 (1.25)	28.90 (1.18)	0.76; 0.30
ADNI memory	1.20 (0.62)	1.02 (0.62)	0.27; 1.12
ADNI executive function	0.85 (0.65)	0.63 (0.58)	0.18; 1.37

Aβ −ve, amyloid beta negative; Aβ +ve, amyloid beta positive; ADAS, Alzheimer's disease assessment scale; MMSE, Mini-mental state examination; ADNI memory, composite memory score from the Alzheimer's disease neuroimaging initiative; ADNI executive function, composite executive function score from the Alzheimer's disease neuroimaging initiative.

General Electric medical systems scanners were used. Furthermore, site was included as a covariate. All ADNI participants provided informed written consent approved by each sites' Institutional Review Board.

2.2 | Amyloid beta PET imaging

Image data underwent a standardized preprocessing procedure at the ADNI project to increase data uniformity. Participant-level amyloid beta (Aβ) standardized uptake value ratios were calculated as the average of the uptake values of the frontal, angular/posterior cingulate, lateral parietal, and temporal cortices divided by the mean uptake values of the cerebellum, following a standardized pipeline (ADNI, 2011; Landau et al., 2013). Baseline Aβ positivity (+ve/−ve) was derived using standardized uptake value ratio cut-off of 1.11 as described previously (Landau et al., 2014). Of the 72 participants included in our study, 21 were Aβ +ve.

2.3 | MR imaging acquisition

All participants underwent whole-brain MRI scans according to ADNI protocol using the same type of 3 T GE Medical Systems scanner across 14 sites. The T1-weighted accelerated sagittal inversion-recovery spoiled gradient-recalled (IR-SPGR) sequence comprised the following parameters: repetition time = 6.96 ms, echo time = 2.8 ms, inversion time = 400 ms, flip angle = 11°, matrix size = 256 × 256 and voxel size = 1.01 × 1.01 × 1.2 mm^3. Axial diffusion-weighted image data were acquired from all participants with a spin echo planar imaging sequence. Scan parameters included: acquisition matrix = 256 × 256, voxel size = 1.4 × 1.4 × 2.7 mm^3, flip angle = 90°, number of slices = 59, 41 diffusion-weighted images (b = 1,000 s/mm^2) and 5 nondiffusion-weighted images (b = 0 s/mm^2). Repetition time varied across scanning sites, but was approximately 12,500 to 13,000 ms.

2.4 | MR image preprocessing

Structural and diffusion images were preprocessed using FreeSurfer (https://surfer.nmr.mgh.harvard.edu, software version 5.3). For each participant's T1 images, automated segmentation and cortical parcellation was carried out using the FreeSurfer "recon-all" processing stream (Desikan et al., 2006; Fischl et al., 2002; Fischl, Salat et al., 2004; Fischl, van der Kouwe et al., 2004), which included motion correction, removal of nonbrain tissue, automated Talairach transformation, intensity correction, volumetric segmentation, and cortical surface reconstruction and parcellation. The FreeSurfer gray matter volume estimations were done in two different ways: (a) using FreeSurfer default automated settings and (b) using manually edited brain and white matter masks. These cross-sectionally processed images were subsequently run through the longitudinal stream in FreeSurfer. In this step, an unbiased within-participant template volume was created for each participant, and processing of all time points was then carried out using common information from this template, thus increasing sensitivity and robustness of the longitudinal analysis (Reuter, Schmansky, Rosas, & Fischl, 2012). Hippocampal, gray matter volume and white matter volume were extracted for each participant at each time point using the Freesurfer recon-all segmentation step.

For DTI image analyses, TRActs Constrained by UnderLying Anatomy (TRACULA), part of FreeSurfer version 5.3, was used to preprocess the DTI data (including eddy-current compensation, motion correction, registration, white matter mask creation, and tensor fitting) and reconstruct 18 major white matter tracts of interest (Yendiki et al., 2011). These 18 fibers comprise a representative labeling of all important established white matter pathways in the brain as recognized in previous literature. This is a novel algorithm for automated global probabilistic tractography that estimates the posterior probability of each pathway given the diffusion-weighted data. The posterior probability is decomposed into a data likelihood term, which uses the "ball-and-stick" model of diffusion (Behrens, Berg, Jbabdi, Rushworth, & Woolrich, 2007), and a pathway prior term, which incorporates prior anatomical knowledge on the pathways from a set of training participants. The segmentation labels required by TRACULA were obtained by processing the T1-weighted images of the study participants as described above. The longitudinal version of TRACULA was used for our study, which computes the joint posterior probability of each pathway given the diffusion MRI data and anatomical segmentations of multiple time points at once. This has been shown to reduce noise, avoid bias toward any specific time point, ensure spatial correspondence between time points and improve both test–retest reliability and sensitivity to longitudinal white matter changes, when compared to reconstructing the pathways at each time point independently (Storsve, Fjell, Yendiki, & Walhovd, 2016; Yendiki, Reuter, Wilkens, Rosas, & Fischl, 2016).

From each of the reconstructed pathways, average tract-wise and tract-position tensor-based fractional anisotropy (FA) was extracted and subject to statistical analyses. The major 18 fibers included: corpus callosum forceps major; corpus callosum forceps minor; left/right anterior thalamic radiation; left/right cingulum angular bundle; left/right cingulum cingulate gyrus; left/right corticospinal tract; left/right inferior longitudinal fasciculus; left/right superior longitudinal fasciculus parietal; left/right superior longitudinal fasciculus temporal; left/right uncinate fasciculus.

2.5 | Free-water imaging method

To carry out free-water correction on the diffusion-weighted data, eddy-current corrected diffusion MRI data in the participant's native space were fitted to the two-compartment FW model (Pasternak et al., 2009, 2015). Specifically, the diffusion tensor was modeled into a FW compartment and a tissue compartment. The FW compartment represents freely diffusing extracellular water with a fixed diffusivity of 3×10^{-3} mm^2/s (the diffusion coefficient of the FW at body temperature) and the fractional volume of this compartment in each voxel forms the FW map. The tissue compartment is the signal following elimination of FW. It accounts for water molecules in proximity to tissue membranes and is thus thought to be more sensitive to axonal and myelination changes (Metzler-Baddeley, O'Sullivan, Bells, Pasternak, & Jones, 2012). All diffusion maps were aligned to a standard template and averaged across a white matter atlas (Johns Hopkins University white matter atlas) to obtain the mean white matter metrics. Additionally, FW-corrected fractional anisotropy (FAt) and the fractional volume of FW were estimated at each position along the tract. Subsequently, FA, FW, and FAt maps were averaged across the fiber masks obtained from TRACULA for each of the 18 fibers.

2.6 | Statistical analysis

We performed statistical analyses using the linear mixed-effects modeling (Cnaan, Laird, & Slasor, 1997) following our previous approach, for example, (Ng, Lo, Lim, Chee, & Zhou, 2016). The details of the statistical analyses are as follows.

2.6.1 | Longitudinal white matter and cognitive changes

First, the effect of age on longitudinal trajectory of average and fiber-based white matter measures (FW and FAt) and cognition was assessed using linear mixed-effects models (Equation (1)):

$$\begin{aligned} Y_{ij} = {} & \gamma_{0.0} + \gamma_{0.1}(\text{Gender}_j) + \gamma_{0.2}(\text{Education}_j) + \gamma_{0.3}(\text{Site2}_j) \\ & + \gamma_{0.4}(\text{Site3}_j) + \ldots + \gamma_{0.15}(\text{Site14}_j) + \gamma_{0.16}(\text{Age}_j) \\ & + \gamma_{1.0}(\text{Time}_{ij}) + \gamma_{1.1}(\text{Age}_j{*}\text{Time}_{ij}) + \mu_{0j} + \mu_{1j}(\text{Time}_{ij}) + r_{ij} \end{aligned} \quad (1)$$

where Y_{ij} is the diffusion MRI metric or cognitive score of interest for individual *j* at time point *i*. The fixed effects of each explanatory variable on *Y* were denoted by the specific γ_0s and γ_1s. In particular, $\gamma_{1.0}$ and $\gamma_{1.1}$ represent effects due to the longitudinal predictor time (years since baseline visit) and its interaction (*) with baseline age (age at baseline visit). μ_{0j} and μ_{1j} represent individual variability in intercepts and longitudinal slopes (i.e., random effects) and r_{ij} represents the residuals. Additionally, $\gamma_{0.\,n}$, n = 3 to 15 represent the dummy coded predictors of the 14 scan sites which along with gender and years of education were entered as covariates of no interest.

This analysis was first conducted for the mean FA, FW, FAt, and cognitive test scores (mini-mental state examination, ADAS, memory, executive function). The analysis was then repeated for each of the 18 fibers obtained, that is, we built a separate linear mixed-effects model per tract per diffusion MRI metric. For fiber-specific results, significant time or age effects were reported at $p < 0.05$ following False Discovery Rate (FDR) correction for multiple comparisons across 18 fibers and then at a lower uncorrected threshold of $p < 0.05$.

2.6.2 | Aβ moderation on longitudinal changes

Secondly, we evaluated the effect of Aβ burden on longitudinal white matter and cognitive changes. We added Aβ burden as a binary variable (Aβ +ve; Aβ -ve) into the linear mixed-effects model (Equation (2)):

$$\begin{aligned} Y_{ij} = {} & \gamma_{0.0} + \gamma_{0.1}(\text{Gender}_j) + \gamma_{0.2}(\text{Education}_j) + \gamma_{0.3}(\text{Site2}_j) \\ & + \gamma_{0.4}(\text{Site3}_j) + \ldots + \gamma_{0.15}(\text{Site14}_j) + \gamma_{0.16}(A\beta_j) \\ & + \gamma_{0.17}(\text{Age}_j) + \gamma_{0.18}(\text{Age}_j{*}A\beta_j) + \gamma_{1.0}(\text{Time}_{ij}) + \gamma_{1.1}(\text{Age}_j{*}\text{Time}_{ij}) \\ & + \gamma_{1.2}(A\beta_j{*}\text{Time}_{ij}) + \gamma_{1.3}(A\beta_j{*}\text{Age}_j{*}\text{Time}_{ij}) + \mu_{0j} + \mu_{1j}(\text{Time}_{ij}) + r_{ij} \end{aligned} \quad (2)$$

where additional fixed effects were included to assess the influence of Aβ burden and its synergistic effect with baseline age and longitudinal time. We applied this model on the FW, Fat, and FA metrics of the whole white matter as well as white matter fibers that showed a significant time effect (Equation (1)). We also applied the same model on ADAS, mini-mental state examination, memory and executive function scores. All results were reported at FDR corrected for the number of fibers tested and then at a lower threshold of uncorrected $p < 0.05$.

2.6.3 | Spatial degradation gradient analysis

To ascertain whether different parts of the fiber showed differential Aβ burden effects on white matter measures, we conducted position-based spatial analysis for any diffusion MRI metric in any fiber that showed a significant Aβ burden effect. Specifically, along a given fiber, we carried out a linear mixed-effects model (Equation (2)) at each position that overlapped across 75% of all the participants (in the native space).

2.6.4 | Brain-cognition associations

Finally, to investigate associations between white matter changes in fibers that showed an Aβ-dependent baseline or longitudinal effects and cognitive declines, we defined 2 sets of slopes reflecting longitudinal changes in white matter measures ($\beta_{1j.\text{WhiteMatter}}$) and cognition ($\beta_{1j.\text{Cognition}}$). Specifically, the predicted values of each dependent variable (e.g., FW) at each time i and for each participant j was first computed using Equation (1) (excluding r_{ij}). For each participant separately, the predicted values were then regressed on time to obtain the participant-specific slopes (e.g., if the participant had four time points, the regression was done on four predicted FW values). This yielded $\beta_{1j.\text{WhiteMatter}}$, and $\beta_{1j.\text{Cognition}}$, reflecting the longitudinal change in white matter and cognitive measures (ADAS, mini-mental state examination, memory, and executive function), respectively, for each participant. We then carried out linear regression analyses (Equation (3)) to test the association between change in FW/FAt and change in cognition in fibers that showed an effect of Aβ burden across all participants.

$$\beta_{1j.\text{Cognition}} = b_0 + b_1(\text{Age}_j) + b_2(\beta_{1j.\text{WhiteMatter}}) + b_3(\beta_{1j.\text{WhiteMatter}}{*}\text{Age}_j) \quad (3)$$

We also conducted similar regression analyses (Equation (4)) to test the association between baseline FW/FAt and baseline cognition, using only data from each participant's first visit.

$$\text{Cognition} = b_0 + b_1(\text{Age}_j) + b_2(\text{WhiteMatter}_j) + b_3(\text{WhiteMatter}_j{*}\text{Age}_j) \quad (4)$$

All statistical analyses were conducted using R 3.0.3 (R Core Team, 2014) with RStudio (RStudio Team, 2012).

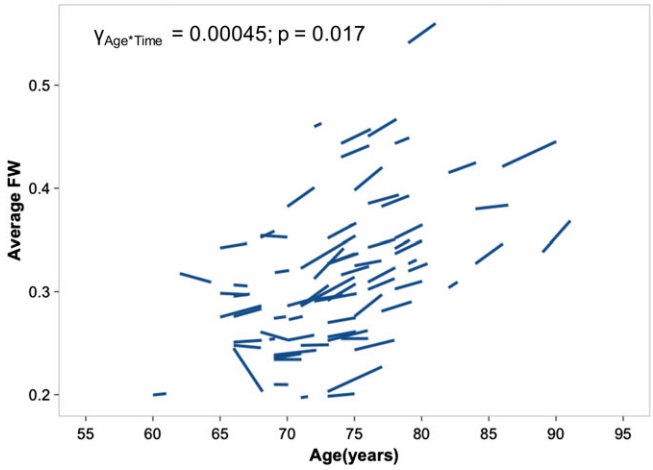

FIGURE 1 Cognitively normal individuals show significant age and time interaction for the average white matter free water. Cognitively normal participants that were older at baseline showed greater increases in FW over time. FW, free water [Color figure can be viewed at wileyonlinelibrary.com]

We repeated all the above the statistical analysis for aging and Aβ effect by including total gray and white matter volume as covariates in Equations (1) and (2). Additionally, we also controlled for hippocampal volume for the assessment of Aβ moderation effect on white matter microstructure by adding hippocampal volume as a covariate in Equation (2) (Supporting Information Supplementary Methods).

3 | RESULTS

3.1 | Aging effect on longitudinal white matter trajectory

3.1.1 | Aging-related alterations in white matter extracellular free-water

For the whole-brain average white matter FW compartment, we found an Age*Time interaction effect across all participants (p = 0.0177; γ = 0.00045; Figure 1) and baseline age (p = 0.0000092; γ = 0.00648) and time (p = 0.0017; γ = 0.00327) effects. Therefore, FW increased over time, while older subjects had higher FW at baseline and steeper FW increase over time.

For fiber-specific FW, eight fibers showed a time effect (Supporting Information Table S1a). Specifically, the right anterior thalamic radiation, right corticospinal tract and left uncinate fasciculus showed significant Age*Time effects at p < 0.05 FDR-correction. Five additional fibers including the right uncinate and inferior longitudinal fasciculus showed trend level Age*Time effects (uncorrected p < 0.05).

All significant results above remained significant following removal of scanner covariates and correction for total gray and white matter volume (Supporting Information Table S1a).

3.1.2 | Aging-related alterations in white matter microstructure

After FW-correction, there were no cross-sectional (age) or longitudinal (time) effects for white matter average FAt. For fiber-specific FAt, the right anterior thalamic radiation showed significant time effect that is, longitudinal decrease, at p < 0.05 FDR-corrected and left cingulum angular bundle and right uncinate fasciculus fibers showed a trend level time effect (uncorrected p < 0.05; Supporting Information Table S1b).

Aging-associated changes in white matter uncorrected FA are summarized in Supporting Information Results 1 and Supporting Information Table S2. Time and Age*Time effects at uncorrected p < 0.05 were observed.

3.2 | The effect of Aβ burden on cross-sectional and longitudinal white matter changes

For whole-brain white matter measures, we did not observe any cross-sectional or longitudinal Aβ effects.

3.2.1 | Aβ burden effect on region-specific extracellular free water

Right inferior longitudinal fasciculus (RILF) FW showed a significant Aβ*Age*Time interaction (p = 0.0061; γ = 0.0031; FDR-corrected p < 0.05). Therefore, in the RILF, Aβ +ve participants with older

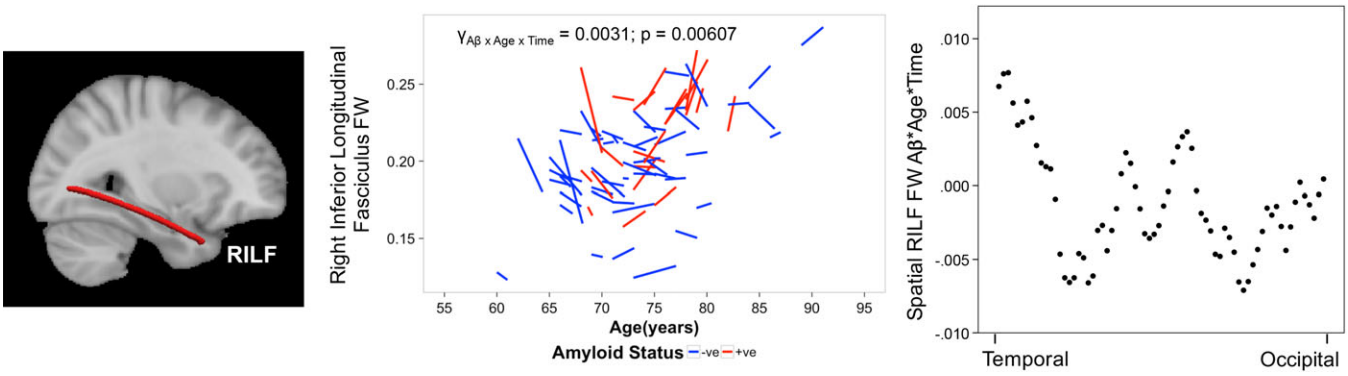

FIGURE 2 Asymptomatic elderly individuals with high amyloid burden exhibit greater longitudinal free water increase in the right inferior longitudinal fasciculus. Brain slice depicts corresponding reconstructed white matter fiber using TRACULA. The spaghetti plot on the left illustrates that cognitively normal elderly participants that were older at baseline and possessed significant Aβ burden in the brain that is, Aβ +ve (red) showed a greater longitudinal increase in the RILF FW over time compared to Aβ −ve participants (blue). The scatterplot on the right illustrates that the spatial Aβ*Age*Time effect (beta value) was higher in the temporal than occipital RILF. Abbreviations: TRACULA, TRActs Constrained by UnderLying Anatomy; FAt, tissue fractional anisotropy; Aβ, amyloid beta; RILF, right inferior longitudinal fasciculus

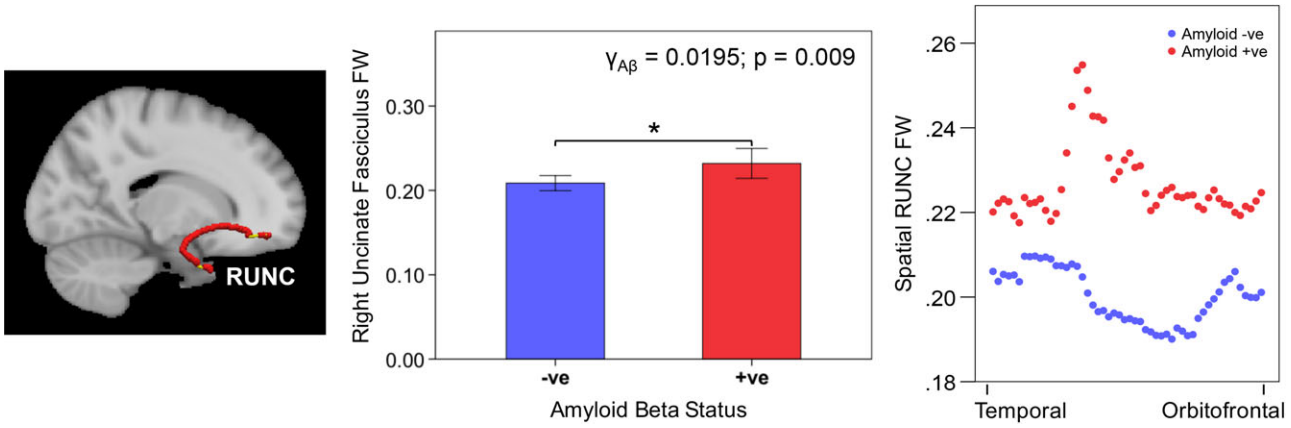

FIGURE 3 Cross-sectional amyloid beta effect on right uncinate fasciculus free water. Brain slices depict corresponding reconstructed white matter fiber using TRACULA. The bar chart on the left illustrates that participants that were Aβ +ve (red) had higher RUNC FW at baseline. Error bars represent ± 2 standard error. The scatterplot on the right illustrates that Aβ +ve participants (red) showed a higher FW than Aβ −ve participants (blue) across all positions in the RUNC, especially in the temporal part of the RUNC. Abbreviations: TRACULA, TRActs Constrained by UnderLying Anatomy; FW, free water; Aβ, amyloid beta; RUNC, right uncinate fasciculus

baseline age showed a steeper FW increase over time than Aβ −ve participants (Figure 2, left). This Aβ-related effect was significant even after removal of scanner covariates and correction for total gray and white matter volume (Supporting Information Table S3a). Spatial analysis indicated larger Aβ*Age*Time effect on FW in the temporal RILF (Figure 2, right).

There was also a cross-sectional Aβ effect on baseline right uncinate fasciculus (RUNC) FW (uncorrected p = 0.0092; γ = 0.0195; FDR-corrected p < 0.10), indicating that Aβ +ve participants had greater RUNC FW at baseline than Aβ –ve participants (Figure 3, left). Spatial analysis revealed higher FW across the entire RUNC in Aβ +ve than Aβ –ve participants, especially in the temporal region of the RUNC (Figure 3, right).

3.2.2 | Aβ burden effect on region-specific FAt

The RUNC FAt showed a significant longitudinal Aβ*Time effect (p = 0.0038; γ = −0.0118; FDR-corrected p < 0.05), i.e., Aβ +ve participants showed greater RUNC FAt reduction over time than Aβ –ve participants (Figure 4, left). Spatial analysis of FAt revealed larger Aβ*Time interactions in the temporal part of the RUNC (Figure 4,right).

RUNC FAt also showed a significant cross-sectional Aβ*Age effect (p = 0.0022; γ = −0.0064; FDR-corrected p < 0.05; Supporting Information Table S3b), i.e., Aβ +ve participants who were older at baseline had lower FAt than Aβ −ve participants.

All these results remained significant following removal of scanner covariates and correction for total gray and white matter volume (Supporting Information Table S3b). We also assessed the influence of continuous Aβ burden on white matter fiber-based measures using baseline AV45 Aβ SUVR values and found similar Aβ-associated effects on white matter microstructure (Supporting Information Results 2; Supporting Information Figure S1).

Aβ-associated changes in uncorrected FA are summarized in the Supporting Information Results 2 (Supporting Information Table S4). No longitudinal effect of Aβ burden was observed for FA.

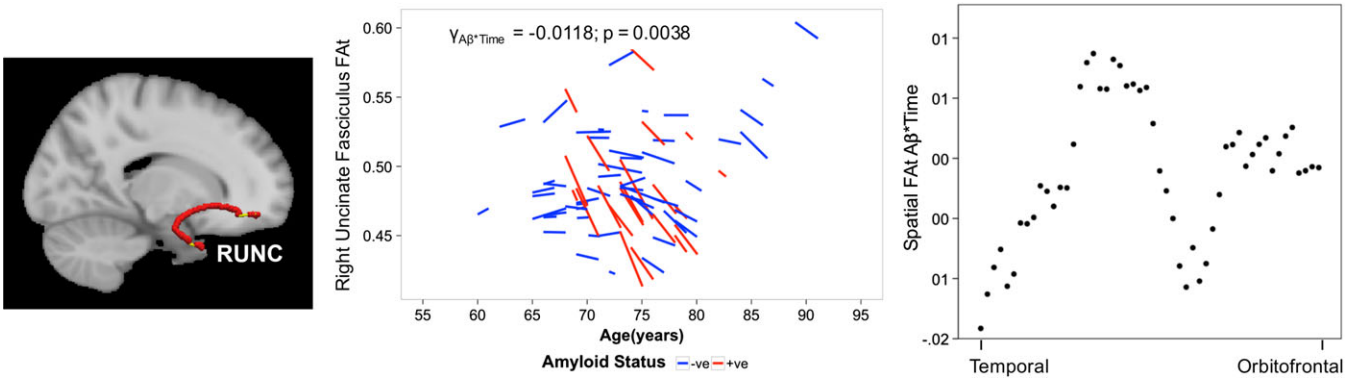

FIGURE 4 Asymptomatic elderly individuals with high amyloid burden exhibit greater longitudinal tissue fractional anisotropy decline in the right uncinate fasciculus. Brain slice depicts corresponding reconstructed white matter fiber using TRACULA. The spaghetti plot on the left illustrates that participants that possessed significant Aβ burden in the brain that is, Aβ +ve (red) showed a greater longitudinal reduction in the RUNC FAt over time compared to Aβ −ve participants (blue). The scatterplot on the right illustrates that the spatial Aβ*Time effect (beta values) was greater in the temporal than orbitofrontal RUNC. Abbreviations: TRACULA, TRActs Constrained by UnderLying Anatomy; FAt, tissue fractional anisotropy; Aβ, amyloid beta; RUNC, right uncinate fasciculus

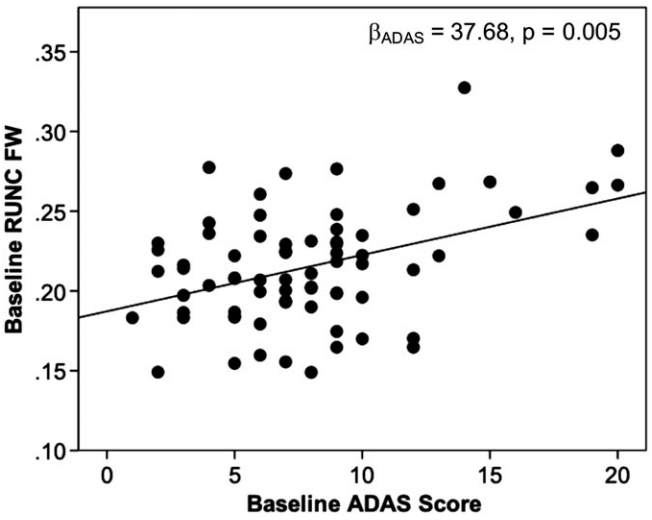

FIGURE 5 Baseline Alzheimer's disease assessment scale score is associated with baseline right uncinate fasciculus free water. With increase in baseline ADAS score there was an increase in RUNC FW at baseline. Abbreviations: RUNC, right uncinate fasciculus; FW, free water; ADAS, Alzheimer's disease assessment scale

3.2.3 | Aβ burden effect on hippocampal volume and its potential influence on white matter trajectory

We also assessed the cross-sectional and longitudinal Aβ effect on hippocampal volume, a region traversed by both uncinate fasciculus (UNC) and inferior longitudinal fasciculus (ILF) fibers (Supporting Information—Supplementary Methods). Right hippocampal volume, but not left hippocampus, showed Aβ-associated reductions over time (p = 0.0056; γ = –0.067) and at baseline (p = 0.012; γ = –0.314). Total hippocampal volume showed a cross-sectional effect of Aβ burden (p = 0.045; γ = –0.505) and longitudinal Aβ*Time effect (p = 0.0071; γ = –0.1013). These Aβ-associated effects on total hippocampal and right hippocampal volume remained significant following correction for total gray and white matter volume. We also assessed the influence of continuous Aβ burden on hippocampal volume using baseline AV45 Aβ SUVR values and observed largely similar effects (Supporting Information Results 3).

Following the above observations, we tested the impact of Aβ burden on white matter microstructure after controlling for hippocampal volume at each time point. Importantly, all main results of Aβ burden on white matter trajectory at baseline and over time remained significant after including total and right hippocampal volume (Supporting Information Results 4).

3.3 | Relationships between cognition, white matter microstructure and Aβ burden

3.3.1 | Aging on cognition

Memory (p = 0.0000073; γ = –0.056), executive function (p = 0.000265; γ = –0.0672), and ADAS (p = 0.000616; γ = 0.323) scores were significantly associated with age at baseline. However, there was no time effect on mini-mental state examination, ADAS, memory or executive function scores.

3.3.2 | Effect of Aβ burden on cognition

We found no baseline or longitudinal effects of Aβ burden on memory, executive function, ADAS, or mini-mental state examination scores.

3.3.3 | Higher baseline ADAS scores were associated with higher baseline RUNC FW while decline in memory scores was associated with increase in RILF FW

Linear regression analyses found that higher ADAS scores were associated with greater RUNC FW at baseline (p = 0.005; b_2 = 37.68; Figure 5).

Longitudinally, the rate of change in RILF FW was associated with change in memory score in an age-dependent manner (p = 0.0306; b_3 = –0.27; Supporting Information Figure S2), suggesting that older participants with greater RILF FW increases over time showed faster memory decline over time. Additionally, decline in hippocampal volume over time was associated with decline in memory scores over time (Supporting Information Results 5).

4 | DISCUSSION

A longitudinal assessment of white matter microstructural changes using free-water imaging revealed differential trajectories between cognitively normal elderly with high versus low Aβ burden. Most strikingly, key AD-related fibers, such as the RUNC and RILF, showed Aβ and age-associated baseline FW increases and Aβ-associated longitudinal FW increases, respectively. Additionally, the RUNC showed Aβ-associated longitudinal FAt decreases. These alterations were more prominent in the temporal region of the RILF and RUNC. Some temporal fibers also showed aging-related FW increases and FAt decreases in the at-risk asymptomatic elderly. Our results highlight that Aβ-associated alterations are evident even in the asymptomatic elderly in white matter fibers known to play critical roles in AD. These findings thus illustrate the potential use of FW-corrected microstructural alterations as biomarkers to indicate key differences in individuals at risk of developing AD and shed more light on disease pathophysiology and progression.

4.1 | Free-water correction helps differentiate between Aβ-associated influence on extracellular and tissue alterations

Our study used the FW-imaging method to assess the trajectory of white matter changes in cognitively normal elderly individuals at-risk of AD. In this regard, it is also important to reiterate that there were no widespread Aβ-related effects on whole-brain white matter measures. Instead, early focal effects of Aβ burden on white matter microstructure decline were observed in our study population of at-risk cognitively normal elderly individuals. Specifically, our investigation found differential changes, especially in the RUNC that can be interpreted as occurring either due to cellular or extracellular changes. While the RUNC showed Aβ-associated higher baseline FW, the RILF showed age and Aβ-associated longitudinal FW increases. There are many potential causes for extracellular changes, however the main

causes comprise cellular density reduction, atrophy, and neuroinflammation (Pasternak et al., 2012). An inflammatory response could be supported by increased cytokine levels, microglial activation and upregulation of inflammatory pathways in AD (Akiyama et al., 2000; Morales, Guzman-Martinez, Cerda-Troncoso, Farias, & Maccioni, 2014). Indeed, Aβ presence in the brain is thought to activate the inflammatory cascade, which may lead to greater extracellular water and associated water compartment changes (Guo, Yu, Grass, de Beer, & Kindy, 2002; Perez-Nievas et al., 2013). We covary gray and white matter volume in order to control for low cell density or low dendritic volume, which may also explain FW changes (Pasternak et al., 2012). Our findings remained significant after controlling for these variables.

We also found Aβ-related longitudinal RUNC FAt reduction. Specifically, regarding this finding's effect size, we observed a significantly greater reduction of 0.05 in FAt value (i.e., 12.5% change) over the 4-year follow-up period in Aβ +ve individuals when compared to Aβ −ve individuals. Since FAt changes originate from tissue itself, it may be better associated with axonal and myelin sheath degeneration (Pasternak et al., 2015). Indeed, reduced Aβ clearance and its influence on blood brain barrier permeability is thought to impact white matter microstructure in prodromal AD, especially in temporal regions such as the hippocampus and parietal areas vulnerable to early Aβ deposition and structural damage (Buckner et al., 2009; Cho et al., 2016; Huang et al., 2012; Iadecola, 2015; Montagne et al., 2015). Cumulatively, such processes may lead to altered homeostasis, inflammation and eventually synaptic dysfunction and cognitive deficits, reflecting a possible mechanism underlying the deleterious influence of high Aβ burden (Iadecola, 2015). Our findings are also congruent with previous studies illustrating distinct Aβ-related blood brain barrier and white matter damage at baseline and over time in preclinical and prodromal phases of AD (Iadecola, 2015; Montagne et al., 2015; Rieckmann et al., 2016). These findings further underscore the importance of the FW-correction method in differentiating tissue-associated from neuroinflammation-associated changes to enable a more precise interpretation of white matter alterations and their trajectory over time (Lyall et al., 2017; Pasternak et al., 2015).

4.2 | White matter fibers implicated in Alzheimer's disease show early signs of impairment in the at-risk cognitively normal elderly

Our results highlighted the Aβ-associated effect on white matter microstructure in RUNC and RILF fibers, known to play important roles in AD development. The UNC links anterior temporal and parahippocampal regions with the medial orbitofrontal cortex, while the ILF links the temporal to the occipital lobe (Remy et al., 2015; Voineskos et al., 2012). Notably, the ILF anteriorly joins the UNC and is considered an indirect pathway that relays information between occipital and orbitofrontal regions (Ashtari, 2012). Associations between UNC and ILF disruptions and cognitive dysfunction in both memory and nonmemory domains have also been observed, reflecting the important role played by these fibers in early disease stages (Kantarci et al., 2011; Liu et al., 2011; Metzler-Baddeley, Hunt, et al., 2012; Voineskos et al., 2012). Indeed, our findings of larger longitudinal Aβ-related effects in temporal RUNC and RILF in the cognitively normal elderly suggest that temporal areas appear to be affected early in Aβ +ve participants. Default mode network regions including the temporal lobe are considered primary sites for early Aβ deposition which might contribute to Aβ-related changes in FW and FAt in white matter fibers traversing these regions (Buckner et al., 2009; Palmqvist et al., 2017). Moreover, recent findings posit a two-phase phenomenon for diffusivity changes in the asymptomatic preclinical AD stage. Similar to the longitudinal RILF FW trajectory illustrated in Aβ +ve subjects in our study, this biphasic model highlights initial FW decreases, followed by FW increases over time (Montal et al., 2017), which might be atrophy-related. Importantly, evidence indicates that Aβ deposition could influence such a trajectory (Racine et al., 2014). Increases in Aβ may initially reduce interstitial extraneuronal spaces (lower FW). However, at later stages Aβ deposition likely influences degeneration and atrophy as illustrated by our FAt reductions over time in Aβ-positive subjects, which then in turn increase extracellular spaces (higher FW; Pasternak et al., 2012). Thus, such a separation between tissue-related and extracellular water related changes can help better to understand the relationship between how changes in various DTI metrics relate to specific protein aggregation related neuropathological changes at various stages along the disease spectrum.

We also observed an Aβ-associated longitudinal decline in right hippocampal gray matter volume only, which could partly influence Aβ-related alterations in temporal RUNC and RILF as revealed in our spatial analysis. Moreover, UNC and ILF damage could be related to anterior medial temporal lobe gray matter atrophy and could begin in the earliest stages of disease (Damoiseaux et al., 2009; Villain et al., 2010). Indeed, Aβ-associated hippocampal gray matter volume reduction is thought to be a causal event in white matter FA reduction in the UNC (Jack Jr. et al., 2014; Sachdev et al., 2013). Thus, a possible temporal sequence of biomarker trajectory in the asymptomatic elderly at-risk of AD could involve early Aβ deposition which then drives early microstructural changes in the UNC and other related fibers like the ILF, closely followed by gray matter atrophy and subsequent cognitive decline as disease sets in (Hong et al., 2015; Sachdev et al., 2013).

Nevertheless, importantly, following hippocampal volume correction at each time point, Aβ-associated effects on both FW and FAt remained significant. Thus, other factors such as neuroinflammation, in addition to gray matter atrophy, may play a role in microstructural alterations (Salat et al., 2010). While hippocampal atrophy is a hallmark of AD, it is unlikely to be holistically representative of Aβ-associated effects. On the other hand, white matter abnormalities, while subtle, are perhaps more informative since they are observed in addition to and disparate from hippocampal atrophy (Hong et al., 2015).

Although cognitive performance declined with increase in baseline age (but not over time), only increase in RILF FW over time and higher baseline age was associated with greater memory decline, and higher ADAS scores were associated with higher RUNC FW. This may suggest potential relationships between Aβ burden, extracellular processes such as neuroinflammation, and cognitive impairment in early disease stages (Hedden, Oh, Younger, & Patel, 2013).

4.3 | Limitations and future directions

While this study provides important insights into early white matter microstructural alterations in the cognitively normal elderly participants at-risk of AD, we did not have access to histological or pathological data, and therefore cannot determine the exact cellular mechanisms that link Aβ and white matter diffusion MRI measures. However, current Aβ measurements are invasive (CSF or PET) and our findings shed light on how FW may be a safer potential biomarker for disease progression. Nonetheless, the association between alterations in diffusion parameters and Aβ burden need further investigation and biological studies are required to demonstrate the direct effects of neuropathological protein aggregation on white matter microstructure. The FW-elimination approach is also more accurate with multi-shell diffusion MRI data and future studies should aim at the collection of such longitudinal data. Additionally, it is also likely that some cognitively normal elderly individuals in our cohort, despite having high Aβ burden and being at-risk of AD, may never progress further along the disease spectrum. Thus, longer follow-up acquisition of amyloid-PET, diffusion MRI and neuropsychological assessments with larger sample sizes are imperative to provide greater insight regarding the veracity of our findings and the association between longitudinal white matter measures and cognition and the impact of Aβ burden in individuals at-risk of AD. Moreover, despite using the linear mixed-effects modeling model to take into account factors like age, our study cannot entirely ensure that all asymptomatic individuals were at the same disease stage or subtype. In this regard, studies with larger samples will enable us to use more principled statistical approaches such as hierarchical linear modeling to assess more complex relationships between white matter microstructure trajectories and various disease markers in preclinical AD. Taking into account the effect size of Aβ-related effects on white matter FAt and FW from our model, focusing on specific focal effects such as those occurring in the UNC could be vital in identifying subjects with faster disease progression in later years. Furthermore, future studies could assess the influence of AD pathology such as Aβ burden on all tissue-related DTI metrics including tissue-based fractional anisotropy, axial diffusivity and radial diffusivity simultaneously in a multivariate approach. This could further shed light on joint patterns of white matter microstructure changes induced by AD pathology.

In summary, our study demonstrates the associations of Aβ burden with both cross-sectional and longitudinal white matter microstructural measures in the at-risk cognitively normal elderly. Together with Aβ burden, FW-corrected white matter measures may provide more detailed insight regarding the regions showing early decline prior to symptom onset and their interaction with factors involved in the progression to mild cognitive impairment or AD. Collectively, our study underlines the importance of longitudinally examining asymptomatic elderly individuals to help decipher changes in the brain that could contribute to early disease detection such that corrective measures can be taken before irreversible damage occurs.

ACKNOWLEDGMENTS

Data collection and sharing for this project was funded by the Alzheimer's Disease Neuroimaging Initiative (ADNI) (National Institutes of Health Grant U01 AG024904) and DOD ADNI (Department of Defense award number W81XWH-12-2-0012). ADNI is funded by the National Institute on Aging, the National Institute of Biomedical Imaging and Bioengineering, and through generous contributions from the following: AbbVie, Alzheimer's Association; Alzheimer's Drug Discovery Foundation; Araclon Biotech; BioClinica, Inc.; Biogen; Bristol-Myers Squibb Company; CereSpir, Inc.; Cogstate; Eisai Inc.; Elan Pharmaceuticals, Inc.; Eli Lilly and Company; EuroImmun; F. Hoffmann-La Roche Ltd and its affiliated company Genentech, Inc.; Fujirebio; GE Healthcare; IXICO Ltd.; Janssen Alzheimer Immunotherapy Research & Development, LLC.; Johnson & Johnson Pharmaceutical Research & Development LLC.; Lumosity; Lundbeck; Merck & Co., Inc.; Meso Scale Diagnostics, LLC.; NeuroRx Research; Neurotrack Technologies; Novartis Pharmaceuticals Corporation; Pfizer Inc.; Piramal Imaging; Servier; Takeda Pharmaceutical Company; and Transition Therapeutics. The Canadian Institutes of Health Research is providing funds to support ADNI clinical sites in Canada. Private sector contributions are facilitated by the Foundation for the National Institutes of Health (www.fnih.org). The grantee organization is the Northern California Institute for Research and Education, and the study is coordinated by the Alzheimer's Therapeutic Research Institute at the University of Southern California. ADNI data are disseminated by the Laboratory for Neuro Imaging at the University of Southern California. We would like to thank all participants for their participation in this study. Data analyses for this research was supported by the Biomedical Research Council, Singapore (BMRC 04/1/36/372), National Medical Research Council [NMRC0088/2015], Duke-NUS Medical School Signature Research Program funded by Ministry of Health, Singapore, awarded to JZ, as well as National Institutes of Health grants P41 EB015902, awarded to OP.

CONFLICT OF INTEREST

The authors have no potential conflicts of interest.

ORCID

Juan Helen Zhou https://orcid.org/0000-0002-0180-8648

REFERENCES

Adluru, N., Destiche, D. J., Lu, S. Y., Doran, S. T., Birdsill, A. C., Melah, K. E., … Bendlin, B. B. (2014). White matter microstructure in late middle-age: Effects of apolipoprotein E4 and parental family history of Alzheimer's disease. *Neuroimage Clinical*, *4*, 730–742.

ADNI. (2011). *ADNI 2 PET Technical Procedures Manual AV-45 (Florbetapir F 18) & FDG*. Boston, MA: ADNI.

Akiyama, H., Barger, S., Barnum, S., Bradt, B., Bauer, J., Cole, G. M., … Wyss-Coray, T. (2000). Inflammation and Alzheimer's disease. *Neurobiology of Aging*, *21*, 383–421.

Alzheimer Disease Neuroimaging Initiative. (2008). *ADNI 2 Procedures Manual*. Boston, MA: ADNI.

Ashtari, M. (2012). Anatomy and functional role of the inferior longitudinal fasciculus: A search that has just begun. *Developmental Medicine and Child Neurology*, *54*, 6–7.

Assaf, Y., & Pasternak, O. (2008). Diffusion tensor imaging (DTI)-based white matter mapping in brain research: A review. *Journal of Molecular Neuroscience*, *34*, 51–61.

Behrens, T. E., Berg, H. J., Jbabdi, S., Rushworth, M. F., & Woolrich, M. W. (2007). Probabilistic diffusion tractography with multiple fibre orientations: What can we gain? *NeuroImage*, *34*, 144–155.

Buckner, R. L., Sepulcre, J., Talukdar, T., Krienen, F. M., Liu, H., Hedden, T., … Johnson, K. A. (2009). Cortical hubs revealed by intrinsic functional connectivity: Mapping, assessment of stability, and relation to Alzheimer's disease. *The Journal of Neuroscience*, *29*, 1860–1873.

Chao, L. L., Decarli, C., Kriger, S., Truran, D., Zhang, Y., Laxamana, J., … Weiner, M. W. (2013). Associations between white matter hyperintensities and beta amyloid on integrity of projection, association, and limbic fiber tracts measured with diffusion tensor MRI. *PLoS One*, *8*, e65175.

Cho, H., Choi, J. Y., Hwang, M. S., Kim, Y. J., Lee, H. M., Lee, H. S., … Lyoo, C. H. (2016). In vivo cortical spreading pattern of tau and amyloid in the Alzheimer disease spectrum. *Annals of Neurology*, *80*, 247–258.

Cnaan, A., Laird, N. M., & Slasor, P. (1997). Using the general linear mixed model to analyse unbalanced repeated measures and longitudinal data. *Statistics in Medicine*, *16*, 2349–2380.

Damoiseaux, J. S., Smith, S. M., Witter, M. P., Sanz-Arigita, E. J., Barkhof, F., Scheltens, P., … Rombouts, S. A. (2009). White matter tract integrity in aging and Alzheimer's disease. *Human Brain Mapping*, *30*, 1051–1059.

Desikan, R. S., Segonne, F., Fischl, B., Quinn, B. T., Dickerson, B. C., Blacker, D., … Killiany, R. J. (2006). An automated labeling system for subdividing the human cerebral cortex on MRI scans into gyral based regions of interest. *NeuroImage*, *31*, 968–980.

Englund, E., Brun, A., & Alling, C. (1988). White matter changes in dementia of Alzheimer's type. Biochemical and neuropathological correlates. *Brain*, *111*(Pt 6), 1425–1439.

Fischl, B., Salat, D. H., Busa, E., Albert, M., Dieterich, M., Haselgrove, C., … Dale, A. M. (2002). Whole brain segmentation: Automated labeling of neuroanatomical structures in the human brain. *Neuron*, *33*, 341–355.

Fischl, B., Salat, D. H., van der Kouwe, A. J., Makris, N., Segonne, F., Quinn, B. T., & Dale, A. M. (2004). Sequence-independent segmentation of magnetic resonance images. *NeuroImage*, *23*(Suppl 1), S69–S84.

Fischl, B., van der Kouwe, A., Destrieux, C., Halgren, E., Segonne, F., Salat, D. H., … Dale, A. M. (2004). Automatically parcellating the human cerebral cortex. *Cerebral Cortex*, *14*, 11–22.

Ge, Y., Grossman, R. I., Babb, J. S., Rabin, M. L., Mannon, L. J., & Kolson, D. L. (2002). Age-related total gray matter and white matter changes in normal adult brain. Part I: Volumetric MR imaging analysis. *AJNR. American Journal of Neuroradiology*, *23*, 1327–1333.

Gold, B. T., Zhu, Z., Brown, C. A., Andersen, A. H., LaDu, M. J., Tai, L., … Smith, C. D. (2014). White matter integrity is associated with cerebrospinal fluid markers of Alzheimer's disease in normal adults. *Neurobiology of Aging*, *35*, 2263–2271.

Guo, J. T., Yu, J., Grass, D., de Beer, F. C., & Kindy, M. S. (2002). Inflammation-dependent cerebral deposition of serum amyloid a protein in a mouse model of amyloidosis. *The Journal of Neuroscience*, *22*, 5900–5909.

Hedden, T., Oh, H., Younger, A. P., & Patel, T. A. (2013). Meta-analysis of amyloid-cognition relations in cognitively normal older adults. *Neurology*, *80*, 1341–1348.

Hong, Z., Ng, K. K., Sim, S. K., Ngeow, M. Y., Zheng, H., Lo, J. C., … Zhou, J. (2015). Differential age-dependent associations of gray matter volume and white matter integrity with processing speed in healthy older adults. *NeuroImage*, *123*, 42–50.

Huang, H., Fan, X., Weiner, M., Martin-Cook, K., Xiao, G., Davis, J., … Diaz-Arrastia, R. (2012). Distinctive disruption patterns of white matter tracts in Alzheimer's disease with full diffusion tensor characterization. *Neurobiology of Aging*, *33*, 2029–2045.

Iadecola, C. (2015). Dangerous leaks: Blood-brain barrier woes in the aging hippocampus. *Neuron*, *85*, 231–233.

Jack, C. R., Jr., Knopman, D. S., Jagust, W. J., Petersen, R. C., Weiner, M. W., Aisen, P. S., … Trojanowski, J. Q. (2013). Tracking pathophysiological processes in Alzheimer's disease: An updated hypothetical model of dynamic biomarkers. *Lancet Neurology*, *12*, 207–216.

Jack, C. R., Jr., & Vemuri, P. (2018). Amyloid-beta - a reflection of risk or a preclinical marker? *Nature Reviews. Neurology*, *14*, 319–320.

Jack, C. R., Jr., Wiste, H. J., Knopman, D. S., Vemuri, P., Mielke, M. M., Weigand, S. D., … Petersen, R. C. (2014). Rates of beta-amyloid accumulation are independent of hippocampal neurodegeneration. *Neurology*, *82*, 1605–1612.

Ji, F., Pasternak, O., Liu, S., Loke, Y. M., Choo, B. L., Hilal, S., … Zhou, J. (2017). Distinct white matter microstructural abnormalities and extracellular water increases relate to cognitive impairment in Alzheimer's disease with and without cerebrovascular disease. *Alzheimer's Research & Therapy*, *9*, 63.

Kantarci, K., Senjem, M. L., Avula, R., Zhang, B., Samikoglu, A. R., Weigand, S. D., … Jack, C. R., Jr. (2011). Diffusion tensor imaging and cognitive function in older adults with no dementia. *Neurology*, *77*, 26–34.

Landau, S. M., Breault, C., Joshi, A. D., Pontecorvo, M., Mathis, C. A., Jagust, W. J., … Alzheimer Disease Neuroimaging Initiative. (2013). Amyloid-beta imaging with Pittsburgh compound B and florbetapir: Comparing radiotracers and quantification methods. *Journal of Nuclear Medicine*, *54*, 70–77.

Landau, S. M., Thomas, B. A., Thurfjell, L., Schmidt, M., Margolin, R., Mintun, M., … Alzheimer Disease Neuroimaging Initiative. (2014). Amyloid PET imaging in Alzheimer's disease: A comparison of three radiotracers. *European Journal of Nuclear Medicine and Molecular Imaging*, *41*, 1398–1407.

Liu, Y., Spulber, G., Lehtimaki, K. K., Kononen, M., Hallikainen, I., Grohn, H., … Soininen, H. (2011). Diffusion tensor imaging and tract-based spatial statistics in Alzheimer's disease and mild cognitive impairment. *Neurobiology of Aging*, *32*, 1558–1571.

Lovden, M., Kohncke, Y., Laukka, E. J., Kalpouzos, G., Salami, A., Li, T. Q., … Backman, L. (2014). Changes in perceptual speed and white matter microstructure in the corticospinal tract are associated in very old age. *NeuroImage*, *102*(Pt 2), 520–530.

Lyall, A. E., Pasternak, O., Robinson, D. G., Newell, D., Trampush, J. W., Gallego, J. A., … Szeszko, P. R. (2017). Greater extracellular free-water in first-episode psychosis predicts better neurocognitive functioning. *Molecular Psychiatry*, *23*, 701–707.

Maier-Hein, K. H., Westin, C. F., Shenton, M. E., Weiner, M. W., Raj, A., Thomann, P., … Pasternak, O. (2015). Widespread white matter degeneration preceding the onset of dementia. *Alzheimers Dement*, *11*, 485–493.e2.

McKhann, G. M., Knopman, D. S., Chertkow, H., Hyman, B. T., Jack, C. R., Jr., Kawas, C. H., … Phelps, C. H. (2011). The diagnosis of dementia due to Alzheimer's disease: Recommendations from the National Institute on Aging-Alzheimer's Association workgroups on diagnostic guidelines for Alzheimer's disease. *Alzheimers Dement*, *7*, 263–269.

Melah, K. E., Lu, S. Y., Hoscheidt, S. M., Alexander, A. L., Adluru, N., Destiche, D. J., … Bendlin, B. B. (2016). Cerebrospinal fluid markers of Alzheimer's disease pathology and microglial activation are associated with altered white matter microstructure in asymptomatic adults at risk for Alzheimer's disease. *Journal of Alzheimer's Disease*, *50*, 873–886.

Metzler-Baddeley, C., Hunt, S., Jones, D. K., Leemans, A., Aggleton, J. P., & O'Sullivan, M. J. (2012). Temporal association tracts and the breakdown of episodic memory in mild cognitive impairment. *Neurology*, *79*, 2233–2240.

Metzler-Baddeley, C., O'Sullivan, M. J., Bells, S., Pasternak, O., & Jones, D. K. (2012). How and how not to correct for CSF-contamination in diffusion MRI. *NeuroImage*, *59*, 1394–1403.

Molinuevo, J. L., Ripolles, P., Simo, M., Llado, A., Olives, J., Balasa, M., … Rami, L. (2014). White matter changes in preclinical Alzheimer's disease: A magnetic resonance imaging-diffusion tensor imaging study on cognitively normal older people with positive amyloid beta protein 42 levels. *Neurobiology of Aging*, *35*, 2671–2680.

Montagne, A., Barnes, S. R., Sweeney, M. D., Halliday, M. R., Sagare, A. P., Zhao, Z., … Zlokovic, B. V. (2015). Blood-brain barrier breakdown in the aging human hippocampus. *Neuron*, *85*, 296–302.

Montal, V., Vilaplana, E., Alcolea, D., Pegueroles, J., Pasternak, O., Gonzalez-Ortiz, S., … Fortea, J. (2017). Cortical microstructural changes along the Alzheimer's disease continuum. *Alzheimer's & Dementia*, *14*(3), 340–351.

Morales, I., Guzman-Martinez, L., Cerda-Troncoso, C., Farias, G. A., & Maccioni, R. B. (2014). Neuroinflammation in the pathogenesis of Alzheimer's disease. A rational framework for the search of novel therapeutic approaches. *Frontiers in Cellular Neuroscience*, *8*, 112.

Ng, K. K., Lo, J. C., Lim, J. K. W., Chee, M. W. L., & Zhou, J. (2016). Reduced functional segregation between the default mode network and the executive control network in healthy older adults: A longitudinal study. *NeuroImage*, *133*, 321–330.

Palmqvist, S., Scholl, M., Strandberg, O., Mattsson, N., Stomrud, E., Zetterberg, H., … Hansson, O. (2017). Earliest accumulation of

beta-amyloid occurs within the default-mode network and concurrently affects brain connectivity. *Nature Communications*, *8*, 1214.

Pasternak, O., Sochen, N., Gur, Y., Intrator, N., & Assaf, Y. (2009). Free water elimination and mapping from diffusion MRI. *Magnetic Resonance in Medicine*, *62*, 717–730.

Pasternak, O., Westin, C. F., Bouix, S., Seidman, L. J., Goldstein, J. M., Woo, T. U., … Kubicki, M. (2012). Excessive extracellular volume reveals a neurodegenerative pattern in schizophrenia onset. *The Journal of Neuroscience*, *32*, 17365–17372.

Pasternak, O., Westin, C. F., Dahlben, B., Bouix, S., & Kubicki, M. (2015). The extent of diffusion MRI markers of neuroinflammation and white matter deterioration in chronic schizophrenia. *Schizophrenia Research*, *161*, 113–118.

Perez-Nievas, B. G., Stein, T. D., Tai, H. C., Dols-Icardo, O., Scotton, T. C., Barroeta-Espar, I., … Gomez-Isla, T. (2013). Dissecting phenotypic traits linked to human resilience to Alzheimer's pathology. *Brain*, *136*, 2510–2526.

R Core Team. (2014). *R: A language and environment for statistical computing*. Vienna, Austria: R Foundation for Statistical Computing.

Rabinovici, G. D., & Jagust, W. J. (2009). Amyloid imaging in aging and dementia: Testing the amyloid hypothesis in vivo. *Behavioural Neurology*, *21*, 117–128.

Racine, A. M., Adluru, N., Alexander, A. L., Christian, B. T., Okonkwo, O. C., Oh, J., … Johnson, S. C. (2014). Associations between white matter microstructure and amyloid burden in preclinical Alzheimer's disease: A multimodal imaging investigation. *Neuroimage Clinical*, *4*, 604–614.

Remy, F., Vayssiere, N., Saint-Aubert, L., Barbeau, E., & Pariente, J. (2015). White matter disruption at the prodromal stage of Alzheimer's disease: Relationships with hippocampal atrophy and episodic memory performance. *Neuroimage Clinical*, *7*, 482–492.

Reuter, M., Schmansky, N. J., Rosas, H. D., & Fischl, B. (2012). Within-subject template estimation for unbiased longitudinal image analysis. *NeuroImage*, *61*, 1402–1418.

Rieckmann, A., Van Dijk, K. R., Sperling, R. A., Johnson, K. A., Buckner, R. L., & Hedden, T. (2016). Accelerated decline in white matter integrity in clinically normal individuals at risk for Alzheimer's disease. *Neurobiology of Aging*, *42*, 177–188.

RStudio Team. (2012). *RStudio: Integrated development environment for R*. Boston, MA: RStudio, Inc.

Sachdev, P. S., Zhuang, L., Braidy, N., & Wen, W. (2013). Is Alzheimer's a disease of the white matter? *Current Opinion in Psychiatry*, *26*, 244–251.

Salat, D. H., Tuch, D. S., van der Kouwe, A. J., Greve, D. N., Pappu, V., Lee, S. Y., … Rosas, H. D. (2010). White matter pathology isolates the hippocampal formation in Alzheimer's disease. *Neurobiology of Aging*, *31*, 244–256.

Sojkova, J., & Resnick, S. M. (2011). In vivo human amyloid imaging. *Current Alzheimer Research*, *8*, 366–372.

Sperling, R. A., Aisen, P. S., Beckett, L. A., Bennett, D. A., Craft, S., Fagan, A. M., … Phelps, C. H. (2011). Toward defining the preclinical stages of Alzheimer's disease: Recommendations from the National Institute on Aging-Alzheimer's Association workgroups on diagnostic guidelines for Alzheimer's disease. *Alzheimers Dement*, *7*, 280–292.

Storsve, A. B., Fjell, A. M., Yendiki, A., & Walhovd, K. B. (2016). Longitudinal changes in white matter tract integrity across the adult lifespan and its relation to cortical thinning. *PLoS One*, *11*, e0156770.

Vernooij, M. W., Ikram, M. A., Vrooman, H. A., Wielopolski, P. A., Krestin, G. P., Hofman, A., … Breteler, M. M. (2009). White matter microstructural integrity and cognitive function in a general elderly population. *Archives of General Psychiatry*, *66*, 545–553.

Villain, N., Fouquet, M., Baron, J. C., Mezenge, F., Landeau, B., de La Sayette, V., … Chetelat, G. (2010). Sequential relationships between grey matter and white matter atrophy and brain metabolic abnormalities in early Alzheimer's disease. *Brain*, *133*, 3301–3314.

Voineskos, A. N., Rajji, T. K., Lobaugh, N. J., Miranda, D., Shenton, M. E., Kennedy, J. L., … Mulsant, B. H. (2012). Age-related decline in white matter tract integrity and cognitive performance: A DTI tractography and structural equation modeling study. *Neurobiology of Aging*, *33*, 21–34.

Wang, Y., West, J. D., Flashman, L. A., Wishart, H. A., Santulli, R. B., Rabin, L. A., … Saykin, A. J. (2012). Selective changes in white matter integrity in MCI and older adults with cognitive complaints. *Biochimica et Biophysica Acta*, *1822*, 423–430.

Yendiki, A., Panneck, P., Srinivasan, P., Stevens, A., Zollei, L., Augustinack, J., … Fischl, B. (2011). Automated probabilistic reconstruction of white-matter pathways in health and disease using an atlas of the underlying anatomy. *Frontiers in Neuroinformatics*, *5*, 23.

Yendiki, A., Reuter, M., Wilkens, P., Rosas, H. D., & Fischl, B. (2016). Joint reconstruction of white-matter pathways from longitudinal diffusion MRI data with anatomical priors. *NeuroImage*, *127*, 277–286.

SUPPORTING INFORMATION

Additional supporting information may be found online in the Supporting Information section at the end of the article.

How to cite this article: Vipin A, Ng KK, Ji F, et al. Amyloid burden accelerates white matter degradation in cognitively normal elderly individuals. *Hum Brain Mapp*. 2019;1–11. https://doi.org/10.1002/hbm.24507